

COMSOL[®] Implementation of a viscoelastic model with cure-temperature-time superposition for predicting cure stresses and springback in a thermoset resin

Bhaskar Patham

General Motors Global Research and Development, India Science Lab, GM Technical Centre India Pvt. Ltd., ITPL, Whitefield Rd., Bangalore 560066, INDIA; bhaskar.patham@gm.com

Abstract: Multi-physics simulations of the evolution of cure induced stresses in a viscoelastic thermoset polymeric resin are presented. The viscoelastic material model is implemented with a relaxation spectrum with 34 relaxation time constants. The trends in viscoelastic stresses at different degrees of cure and temperatures are compared and contrasted with an equivalent cure-dependent (but time-invariant) elastic material model. The material models are implemented in the context of the cure of a thick thermoset resin part, to explore the combined effect of multiple phenomena – mold-part interaction, cure shrinkage strains, thermal strains, and the exothermic heat of reaction resulting in a two way coupling between heat transfer and chemical kinetics – on the evolution of residual stresses and springback.

1. Introduction

Accurate predictions of residual stresses in thermoset resins, adhesives, and composites require detailed accounting of multiple phenomena – mold-part interaction, cure shrinkage strains, and thermal strains, the kinetics of resin cure, and the evolution of the resin properties with temperature and degree of cure. Residual stress development and shape distortions in thick thermoset sections are further influenced by large temperature gradients across the thickness driven by the exothermic heat of reaction. The resin modulus, a key parameter governing the magnitude of residual stresses, is a strong function of the degree of cure (α) and the temperature history. The curing resin also displays time dependent stress relaxation, governed by intrinsic relaxation times that are functions of the degree of cure and the temperature [1]. In this report, the simulations of evolution of cure-induced residual stresses and springback in a thick thermoset section are presented. The cure- and temperature-dependence of the viscoelastic stresses are modeled by employing an empirical cure-temperature-time superposition scheme (described in Eom et al., [2]) that accounts for

the chemo-thermo-rheological complexity of the curing resin (different mechanisms of stress relaxation prior to and post gelation). Diffusion limited regimes in the cure kinetics of the thermoset are also accounted for in this scheme.

2. Problem Definition

Geometry and Boundary Conditions: The geometry and thermo-mechanical boundary conditions for the simulation are shown in Figure 1:

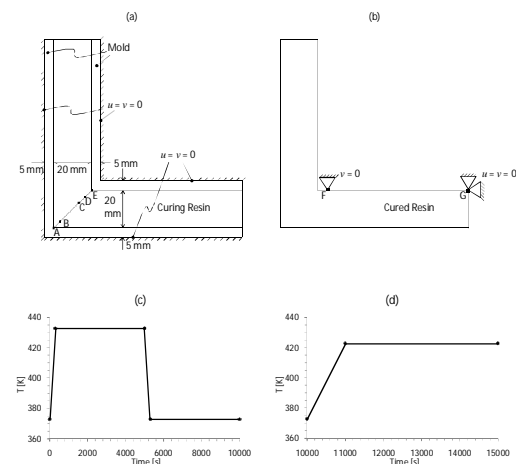


Figure 1: This simulation is implemented in two stages: (I) the first stage involves the cure of a 2 cm thick thermoset in the shape of a right-angled elbow, with the longer (outer) dimension of each arm 10 cm, under constraint between two 5 mm thick structural steel molds (Figure 1a) – to study the evolution of residual stress, using the thermal cycle shown in Figure 1c; (II) the second stage involves the re-heating of the cured elbow geometry (after removal of the molds) under point constraints (Figure 1b), using the thermal cycle shown in Figure 1d - to explore springback effects. The evolution of temperature, cure, and stresses are investigated along the diagonal traversing the thickest portion of the thermoset resin in the elbow geometry at the points **A** (0,0) –**B** (0.0025,0.0025) –**C** (0.01358,0.01358) –**D** (0.0175,0.0175) –**E** (0.02, 0.02), (refer to Figure 1a).

Cure Kinetics: The kinetics of the cure of this resin system [2] is characterized by two distinct regimes: the autocatalytic model, valid in the

conversion (α) range 0 – 0.5, is given as:

$$\frac{d\alpha}{dt} = \left(K_1 + K_2 \alpha^{m_a} \right) (1 - \alpha)^{n_a} \quad (1)$$

$$K_1 = K_{01} \exp\left(\frac{-E_{01}}{RT}\right); K_2 = K_{02} \exp\left(\frac{-E_{02}}{RT}\right) \quad (2)$$

K_1 and K_2 are the rate constants and E_{01} and E_{02} are the Arrhenius activation energies associated with K_1 and K_2 respectively. The n^{th} -order model, applicable at higher conversions ($\alpha > 0.5$), is given as:

$$\frac{d\alpha}{dt} = K_{eff} (1 - \alpha)^n \quad (3)$$

In the above expression, n is the reaction order. K_{eff} is the overall effective reaction rate constant that takes into account both chemical and diffusion aspects that control the kinetics at high conversions (cf. [2]). K_{eff} is given as,

$$K_{eff} = \frac{K}{1 + \exp[C(\alpha - \alpha_c)]}; K = K_0 \exp\left(\frac{-E_0}{RT}\right) \quad (4)$$

K is the rate constant for chemical kinetics (non diffusion-controlled), C is a constant, and α_c is a critical conversion above which diffusive effects come into play. E_0 is the activation energy associated with K . Eom et al.'s estimates [2] for these kinetic parameters for the epoxy-amine resin system are listed in Table 1. The simulated evolution of conversion as a function of time for isothermal cure of the epoxy-amine system is plotted in Figure 2 at different isothermal cure temperatures. It can be seen that diffusion effects (as quantified by n and α_c) prevent the cure reaction from reaching completion, and the final degree of cure shows progressive decrease with reduction of cure temperatures.

Heat Transfer: The conductive heat transfer within the structural steel molds is defined as shown below.

$$\rho C_p \frac{\partial T}{\partial t} - \nabla \cdot (k \cdot \nabla T) = 0 \quad (\text{mold}) \quad (5)$$

In the above equation, ρ , C_p , and k are respectively the density, specific heat, and thermal conductivity of the material. The conductive heat transfer within the curing resin accounts for the heat generation due to the exothermic heat of reaction $\Delta H_{reaction}$ (Table 2).

$$\rho C_p \frac{\partial T}{\partial t} - \nabla \cdot (k \cdot \nabla T) = \rho \Delta H_{reaction} \frac{d\alpha}{dt} \quad (\text{resin}) \quad (6)$$

Table 1. Kinetic parameters for isothermal cure of epoxy-amine resin system (From Eom et al. [2])

Parameter	Value
Autocatalytic Model (Conversion range 0.0 – 0.5)	
K_{01} [1/s]	2.7321×10^5
K_{02} [1/s]	3.8231×10^5
E_{01} [J/mol]	7.2776×10^4
E_{02} [J/mol]	6.6934×10^4
m_a	1.07
n_a	2.43
Nth-Order Model (Conversion range 0.5 – 1.0)	
K_0 [1/s]	29.10
E_0 [J/mol]	3.58×10^4
n	$-0.0403 \times T[\text{K}] + 19.48$
C	69
α_c	$0.0092 \times T[\text{K}] - 3.14$

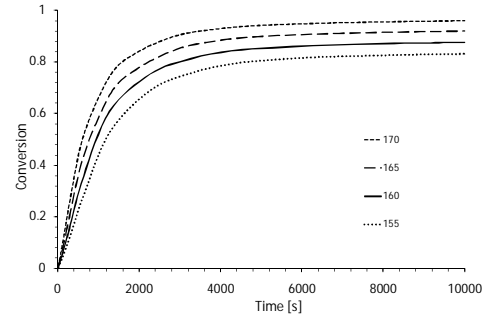


Figure 2: Calculated conversion of epoxy under isothermal curing conditions at four isothermal cure temperatures ($^{\circ}\text{C}$, indicated in the legend)

Table 2. Properties of the resin employed for calculation of cure-induced stresses¹

Density [kg / m ³]	ρ	1.2×10^3
Specific Heat [J/kg-K]	C_p	1.25×10^3
Heat of Reaction [J/mol]	$\Delta H_{reaction}$	100000
Thermal Conductivity [W/m-K]	k	0.2
Poisson's Ratio	ν	0.4
CLTE [ppm/K]	χ	100
Total Specific Volumetric Cure Shrinkage	$\Delta V_{shrinkage}$	-0.06

¹These values are typical of epoxy resins (e.g., [3, 4])

Table 3. Properties of structural steel [5]

Density [kg / m ³]	ρ	7.85×10^3
Specific Heat [J / kg K]	C_p	475
Thermal Conductivity [W/m-K]	k	44.5
Young's Modulus [GPa]	E	200
Poisson's Ratio	ν	0.33
CLTE [ppm / K]	χ	12.3

Structural Mechanics: Assuming the body forces to be negligible, the momentum balance:

$$\nabla \cdot \sigma = 0 \quad (7)$$

was implemented in the geometry shown in Figure 1 using the plane strain approximation, in which the geometry is considered infinitely long in z - (3-) direction, thereby making it possible to ignore any normal or shear strains in that direction: $\varepsilon_{33} = \varepsilon_{23} = \varepsilon_{13} = 0$. The overall stress, $\boldsymbol{\sigma}$, has contributions from an isotropic (pressure) component, p , and a deviatoric stress component, $\boldsymbol{\tau}$.

$$\boldsymbol{\sigma} = \boldsymbol{\tau} - p\mathbf{I} \quad (8)$$

The isotropic component of the stress is defined in terms of the bulk modulus, k , and isotropic strains:

$$p = -k \cdot \text{trace}(\boldsymbol{\varepsilon}) = -k \cdot (\varepsilon_{11} + \varepsilon_{22} + \varepsilon_{33}) \quad (9)$$

The deviatoric strains are defined as:

$$\boldsymbol{\varepsilon}_{deviatoric} = \boldsymbol{\varepsilon} - \frac{1}{3} \text{trace}(\boldsymbol{\varepsilon}) \cdot \mathbf{I} \quad (10)$$

The evolution of the isotropic stresses, due to thermal strains (driven by the coefficient of linear thermal expansion, (χ)) in the structural steel molds, is modeled by modifying the pressure term:

$$p(T) = -k \cdot \{\text{trace}(\boldsymbol{\varepsilon}) - 3\chi(T - T_{ref})\} \quad (\text{mold}) \quad (11)$$

For this analysis, the reference temperature for thermal strains was taken to be 373K. On the other hand, the isotropic stresses generated in the thermoset resin are a combination of thermal stresses and those due to chemical shrinkage:

$$p(T, \alpha) = -k \cdot \{\text{trace}(\boldsymbol{\varepsilon}) - 3\chi(T - T_{ref}) - \Delta V_{shrinkage}\} \quad (\text{resin}) \quad (12)$$

The relevant properties of the epoxy resin (cf. [3, 4]) and the structural steel mold [5] are listed in Tables 2 and 3 respectively.

COMSOL Multiphysics[®] implementation of viscoelastic model [6]: The generalized Maxwell model is expressed as a Prony series:

$$G_r(t) = G_0 \left[\mu_\infty + \sum_{i=1}^N \mu_i \exp(-t/\lambda_i) \right] \quad (13)$$

In the above equation, the coefficient μ_i can be considered to be the relative stiffness (G_i represents the absolute stiffness) of the spring in branch i of the generalized Maxwell model.

$$\mu_i \equiv G_i/G_0 ; \mu_\infty \equiv G_\infty/G_0 \quad (14)$$

$$\mu_\infty + \sum_{i=1}^N \mu_i = 1 ; \sum_{i=1}^N G_i + G_\infty = G_0 \quad (15)$$

The components of $\boldsymbol{\tau}$, and the deviatoric strains are then related, by introducing the variable q_i , (equivalent to the extension of the spring in branch i of the generalized Maxwell model).

$$\boldsymbol{\tau} = 2G_0 \left(\mu_\infty \boldsymbol{\varepsilon}_{deviatoric} + \sum_{i=1}^N \mu_i q_i \right) \quad (16)$$

$$\dot{q}_i + \frac{1}{\lambda_i} q_i = \dot{\boldsymbol{\varepsilon}}_{deviatoric} \quad (17)$$

Cure-temperature-time shift model: The viscoelastic properties of the curing thermoset resin were also studied by Eom et al. [2] using isothermal dynamic shear modulus measurements for several degrees of cure, at a given cure temperature. The relaxation time of the resin at any conversion, α , can be calculated by shifting the relaxation times at the reference conversion to the instantaneous conversion.

$$\lambda_{i\alpha T} = A_x \lambda_i \quad (18)$$

The corresponding relaxation of shear modulus in real time, $G_r(t, T, \alpha)$, at different conversions can then be calculated by employing the shifted relaxation times, $\lambda_{i\alpha T}$, in Equation (13). In order to account for the introduction of additional, and significantly different, relaxation mechanisms for the partially cross-linked gel that comes into existence post gel point (compared to the relatively less cross-linked viscous resin that was present up to the onset of gelation,) and also to account for the temperature dependent limiting conversion, the experimental trends in shift factors with respect to the degree of cure and the temperature were then fitted by Eom et al. [2] using two empirical shift models, to account for the two conversion regimes. In the conversion range 0.0 to 0.7 (before gelation,) only the cure-dependence of the shift factors needs to be accounted for, since the shift factors were observed to be temperature invariant:

$$\log A_x = C_1 \alpha + C_2 \quad (19)$$

For the conversion range 0.7 – 1.0, in which gelation effects become dominant, the dependency of the shift factor on both conversion and temperature needs to be accounted for, as shown in Equation (20).

$$\log A_x = A_{gel} H^{(\alpha - \alpha_{gel})} \left((\alpha_f - \alpha) / (\alpha_f - \alpha_{gel}) \right)^{m_s} \quad (20)$$

With the boundary conditions,

$$\log A_x = A_{gel} \text{ at } \alpha = \alpha_{gel} ; \log A_x = 0 \text{ at } \alpha = \alpha_f. \quad (21)$$

The constants C_1 , C_2 , A_{gel} , and H , as well as the definition of the temperature dependent parameters α_f and m_s , as evaluated by Eom et al. are listed in Table 4. In order to account for the growth of G_0 with the degree of cure (cf. Equations (13-15)), Eom et al. [2] modeled the series coefficients of the relaxation spectrum using a phenomenological relationship:

$$G_i = G_{\tau 0} (G_{u0} / G_{\tau 0})^D ; D = [1 - (1 - n_p) B \lambda_i]^{-1/n_p} \quad (22)$$

$G_{\tau 0}$ is the minimum measurable relaxed modulus, G_{u0} is the un-relaxed modulus at the reference conversion, D is a parameter that determines the shape of the relaxation curve (which, in turn, is governed by the relaxation times, λ_i , of the resin), B is a temperature dependent material parameter, and n_p is a material constant. Eom et al. [2] employed different values for parameters in Equation (22) in the conversion ranges before and after gelation. These parameters are also listed in Table 4. G_{∞} was assigned a value of 0.01 Pa. The bulk modulus, k , and the elastic modulus, E of the curing resin are then calculated from the shear relaxation modulus, assuming a constant Poisson's ratio, $\nu = 0.4$, as shown below [7].

$$E(t, T, \alpha) = 2(1+\nu)G_r(t, T, \alpha) \quad (23)$$

$$k(t, T, \alpha) = \frac{2(1+\nu)G_r(t, T, \alpha)}{3(1-2\nu)} \quad (24)$$

Table 4. Parameters for linear viscoelastic model [2]

Parameter	$\alpha: 0.0 - 0.7$	$\alpha: 0.7 - 1.0$
Parameters for evaluation of time-cure-temperature shift factors		
C_1	30.6	---
C_2	-39.7	---
A_{gel}	---	-17.5
H	---	2
α_{gel}	---	0.7
α_f	---	$0.0074 T(K) - 2.32$
m_s	---	$0.0346 T(K) - 14.23$
Parameters for evaluation of series coefficients of the linear viscoelastic model		
G_{∞}	0.01	0.01
$G_{\tau 0}$	1.0×10^{-4}	1.0×10^3
G_{u0}	1×10^4	1.5×10^8
$\log(B)$	$0.1 T(K) - 62.8$	$0.332 T(K) - 149$
n_p	10	22

The viscoelastic material model has been implemented in the current simulation study with 34 relaxation time constants (ranging from 10^{-1} s to 10^{42} s corresponding to limiting cure at 170°C,) as employed by Eom et al. [2]. The master relaxation spectra (G_i, λ_i) evaluated using Equations (18-22), corresponding to the limiting cures at four different temperatures, with the parameters in Table 2, are plotted in Figure 3.

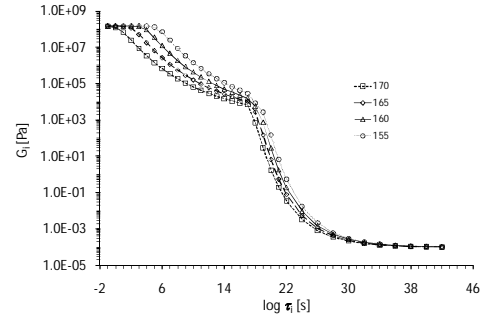


Figure 3: Master relaxation spectra of the epoxy-amine resin system corresponding to the limiting cure at four different temperatures (°C).

Equivalent Elastic Models: In addition to the viscoelastic material model, an equivalent cure- and temperature- dependent (but time invariant) elastic material model was considered, with the magnitude of the elastic shear modulus at any degree of cure set to the value of the viscoelastic shear relaxation modulus at extremely small times, at the same degree of cure.

$$G_{cure_elastic}(T, \alpha) \equiv G_r(t=10^{-12}s, T, \alpha) \quad (25)$$

In this model, only the cure dependence of G_0 is captured. The corresponding cure-dependent elastic bulk and the Young's moduli are calculated using $G_{cure_elastic}(T, \alpha)$ analogously to Equations (23) and (24) respectively.

3. Results and Discussion

The temperature and degree of cure transients in the thermoset resin during the first cure cycle within the mold (refer to Figure 1a, 1c) - at the points A-B-C-D-E - are shown in Figure 4a and 4b respectively. At points A and E, which are in contact with the corners of the structural steel molds, the temperature transients mimic the imposed thermal cycle on the outer surfaces of the molds (Figure 4a). The degree-of-cure transients also evolve similarly at points A and E (Figure 4b). At location B, the enhanced conductive heat transfer to the proximal mold walls in the vicinity of corner A results in temperature and degree of cure transients very similar to those at locations A and E. By contrast, the temperature rise at locations C and D, which are closer to the re-entrant corner E, significantly trails the mold heating cycle (Figure 4a). The progress of cure is also substantially slower at points C and D, compared to A, B or E, for the initial 1000s (Figure 4b). However, as cure progresses, the exothermic heat evolving at C and D cannot be dissipated fast enough (owing to the thickness of the part

and the poor conductive heat removal to the mold walls in the vicinity of E,) and the temperature at these rapidly points rises above that at the mold surface (Figure 4a). At the timescales corresponding to the temperature maximum ($\sim 20^\circ\text{C}$ above the mold temperatures,) the conversion at the locations C and D also shows a rapid increase and exceeds that at the surfaces (Figure 4b). During the cool-down period starting at 5000s, the temperature drop is also slowest at the location C. The final degrees of cure at the various points are dominated by the diffusion controlled limiting conversion corresponding to the hold temperature (Equation (4),) and do not show a very large spread.

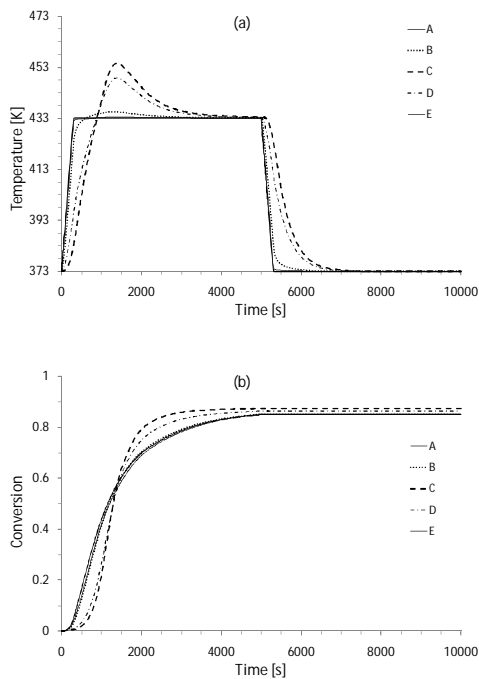


Figure 4: The simulated evolution of (a) temperatures, and (b) degrees of cure, in the thermoset resin at the points A-B-C-D-E during the first cure cycle (cf. Figures 1a, 1c,) within the mold for 10000s

The thermo-chemical residual stress transients within the curing thermoset resin were estimated by the simultaneous FE solutions of the kinetic model, the heat balance, and the momentum balance. In Figure 5a the transients of the maximum principal stress during the first cure cycle within the mold (Figures 1a, 1c), estimated using the elastic material model (cf. Equation (25)) have been plotted at the points A-B-C-D-E (cf. Figure 1a). At location A, the stresses start building up only around 2000s, corresponding to the gel point conversion ($\alpha = \alpha_{gel} = 0.7$) of the thermosetting resin.

Subsequently, as the limiting conversion is attained, the magnitude of the stress stabilizes up to 5000s. Starting at 5000s, during the cool-down phase, the stresses increase once again, due to the onset of constrained thermal shrinkage during cool-down, and stabilize at the final value. While the location A is subjected to the constraining effects of the mold, at the locations B, C, D, and E, the resin is relatively unconstrained; this results in a different evolution of stresses at these locations compared to that at A. For the elastic resin, however, the differences in the evolution of stress transients notwithstanding, since the spatial distribution of the final degree of cure at 10000s is not very broad (refer to Figure 4b), and the temperatures are spatially invariant, the distribution of stresses within the bulk, as demonstrated by the magnitudes of the maximum principal stresses at points B, C, and D, is also relatively narrow.

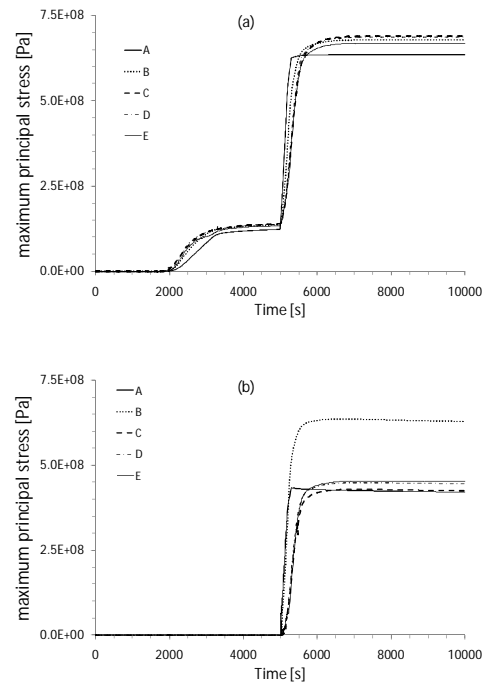


Figure 5: The estimated transients of the maximum principal stress at the points A-B-C-D-E during the first cure cycle (cf. Figures 1a, 1c,) obtained by employing cure- and temperature-dependent (a) linear elastic material model, and (b) viscoelastic material model.

In Figure 5b, the evolution of the maximum principal stresses estimated using the viscoelastic material model have been plotted at the points A-B-C-D-E during the first cure cycle within the mold. In the viscoelastic scenario, all the thermo-chemo-mechanical mechanisms

underlying the development of residual stresses discussed in the context of the elastic material model apply, but additionally, the viscoelastic relaxation of stresses also comes into effect. Comparison of Figures 5a and 5b reveals that accounting for viscoelastic stress relaxation results in significantly lower estimates for stresses compared to those obtained with the linear elastic material model. Even after the onset of gel point (between 2000s and 5000s,) the stresses in the viscoelastic material undergoing cure are insignificant since the relaxation times continue to remain fairly small up to very close to the limiting conversions. Relaxation of the stresses within the core (locations C and D) during the isothermal hold up to 5000s is further expedited by the high temperatures in the core due to the exothermic heat. After 5000s, since the locations C and D cool down much slower than the mold (cf. Figure 4a,) these locations experience significant dwell-times at temperatures which are substantially higher than the mold temperatures; this allows quicker relaxation of stresses brought about by thermal shrinkage, and slower build-up of stresses. However, at the point B, since the cool-down occurs at nearly the same rate as that at the mold, the stresses do not relax as rapidly, and therefore build up faster to a significantly greater value compared to the stresses at C and D (and comparable to that estimated with the elastic material model). Therefore at the end of cure, even though the temperatures are spatially invariant, and the distribution of final degree of cure is not very broad, the distribution of stresses within the bulk, as demonstrated by the magnitudes of the maximum principal stresses at points B, C, and D, is quite broad, owing to the significantly different thermal history at point B compared to those at points C and D.

The contour maps of the maximum principal stresses, estimated with the elastic material model and the linear viscoelastic material model, at the end of the first cure cycle (10000s,) are shown in Figures 6a and 6b respectively. Figures 6a and 6b also show the deformations brought about by the cure of the resin. The edges of the thermoset in contact with the mold are for all practical purposes fully constrained due to the large difference between the coefficients of linear thermal expansion of the mold and the resin. However, the two exposed edges of the curing resin, which are constrained by the steel molds at their end points alone, deform into a concave arc as a result of the

shrinkage strains. The displacements as the result of shrinkage strains in the exposed edges are greater for the viscoelastic material than for the elastic material.

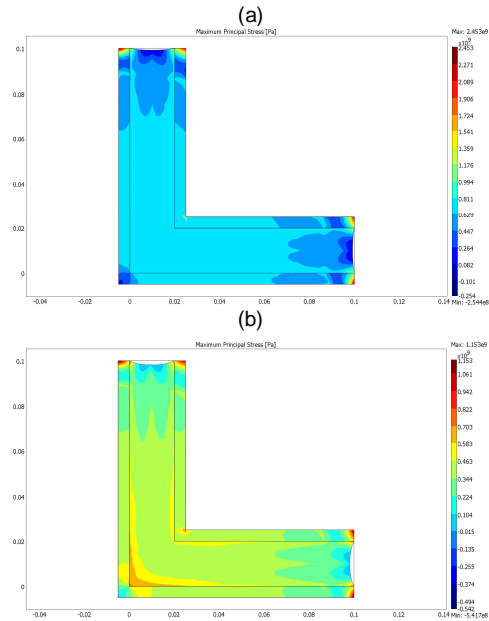


Figure 6: Contour map of the estimated maximum principal stress, and the deformation of the geometry, at the end of the first mold-constrained (cf. Figure 1a, 1c) cure cycle (at 10000s,) estimated by employing cure- and temperature-dependent (a) linear elastic material model, and (b) viscoelastic material model.

As discussed earlier, significant stress gradients along the diagonal of the elbow geometry may be observed in the case of the viscoelastic material (Figure 6b) At the same locations, the stresses in the elastic material, though higher in magnitude, show little variation (Figure 6a). The temperature, cure, and stress distributions, the latter shown in Figure 6, at the end of the first cure cycle provide the initial conditions for the second phase involving the heating of the cured elbow (after removal of the molds,) under point constraints (cf. Figures 1b and 1d). The removal of the molds and the heating would result in the relaxation of the thermo-chemically induced residual stresses that developed under the constraint of the molds during the first phase of curing.

Figure 7a and 7b show the final shapes of the cured resin elbow at the end of the second heating cycle, predicted with cure-dependent elastic and viscoelastic models respectively. Upon removal of the mold constraints, shrinkage of the arms of the elbow is observed with both elastic and viscoelastic material models. In case of the elastic material model (Figure 7a,) the

deformed concave shape of the short edges of the elbow instantaneously straightens out, indicating the release of elastic stored energy upon release of constraints. Moreover, for the elastic material model, in the absence of significant variation in stresses along the diagonal of the elbow (at the end of the first cure cycle), the residual stresses are relieved uniformly across the thickness of the elbow upon removal of constraints; this results in uniform shrinkage across the thickness of the part, and thus there is no shape distortion (or bending).

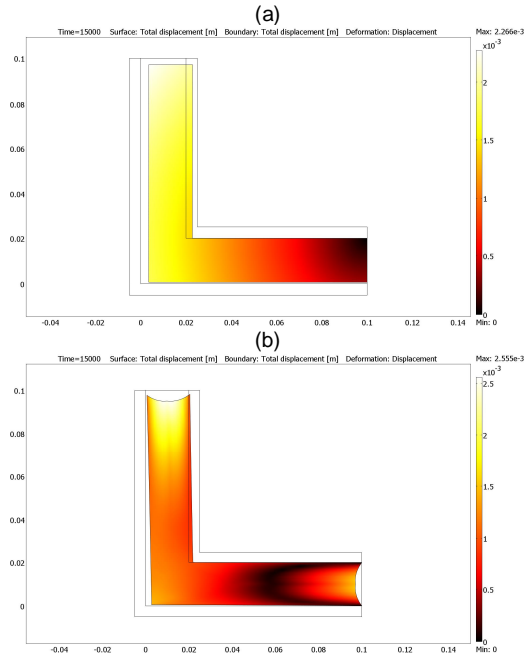


Figure 7: The surface map of total displacement, and the boundary deformation of the cured elbow geometry at the end of the second partially-constrained (cf. Figure 1b, 1d) cure cycle (at 15000s,) estimated by employing (a) linear elastic material model, and (b) viscoelastic material model.

By contrast, as seen in Figure 7b, in case of the viscoelastic material model, the deformed concave shape of the short edges of the elbow is maintained even upon removal of mold constraints and heating, indicating the relatively insignificant magnitudes of elastic stored energy due to viscoelastic relaxation of stresses. Moreover, for the viscoelastic material model, in the presence of large gradients in stresses across the diagonal of the elbow (at the end of the first cure cycle, cf. Figure 6b), the removal of mold constraints results in non-uniform shrinkage across the thickness of the part (with the maximum shrinkage occurring in areas corresponding to the maximum residual stresses), and thus there is significant shape

distortion (or bending) in the viscoelastic material.

SUMMARY

The numerical implementation of the multi-physics problem, involving chemo-thermo-viscoelastic couplings, has been successfully demonstrated in the context of development and relaxation of thermally and crosslink-shrinkage induced stresses during cure of a thick epoxy-amine thermoset section. Phenomenological aspects such as diffusion limited cure kinetics, incomplete cure, the viscoelastic behavior of the resin before as well as after the onset of gelation, and the evolution of the resin relaxation spectrum with the degree of cure have been captured in detail. It is observed from these simulations that while the instantaneous stresses in a linear elastic material are only governed by the instantaneous states of temperature and degree of cure, the stresses in a viscoelastic material are strongly governed by the thermal history experienced by the resin. The spatial gradients in temperature and cure in thick sections (enhanced by the exothermic heat of reaction) can result in significant spatial variation of viscoelastic residual stresses even after equilibration of the temperature fields and achievement of uniform cure; these subtle effects, which have a significant impact on the springback behavior, are not captured by simulations with elastic material models.

ACKNOWLEDGMENTS

The author would like to thank Arun M. Kumar, Hamid Kia, Prakash Mangalgi, Sampath Vanimisetti, and Pete Foss for reviewing this article, and useful discussions.

REFERENCES

1. D. Adolf, and J. E. Martin, *Macromolecules*, **29**, 3700 (1990)
2. Y. Eom, L. Boogh, V. Michaud, P. Sunderland, and J.-A. Manson, *Polymer Engineering and Science*, **40**(6), 1281 (2000)
3. T. A. Bogetti, and J. W. Gillespie Jr., *Journal of Composite Materials*, **26**, 626 (1992)
4. L. G. Zhao, N. A. Warrior, and A. C. Long, *Materials Science and Engineering A*, 452–453, 483 (2007)
5. COMSOL® 3.5a Property Material Database
6. *COMSOL Multiphysics Structural Mechanics Module Model Library*, Version **3.4**, p 443 (2007)
7. S. P. Timoshenko, and J. N. Goodier, *Theory of Elasticity*, Third Edition, McGraw Hills International Edition, Singapore (1970)